Journal of Macromolecular Science, Part A
Publication details, including instructions for authors and subscription information:
http://www.informaworld.com/smpp/title~content=t713597274

Impact of Nanosilicates on Poly(vinylidene fluoride) Crystal Polymorphism: Part 2. Melt-crystallization at Low Supercooling

B. Seyhan Ince-Gunduz[a]; Kristina Burke[b]; Michelle Koplitz[c]; Matthew Meleski[b]; Ari Sagiv[d]; Peggy Cebe[a]
[a] Department of Physics and Astronomy, Tufts University, Medford, MA [b] Department of Chemistry, Gallaudet University, Washington, DC [c] Biology Department, Rochester Institute of Technology, Rochester, NY [d] Department of Materials Science and Engineering, Drexel University, Philadelphia, PA

Online publication date: 12 October 2010

To cite this Article Ince-Gunduz, B. Seyhan , Burke, Kristina , Koplitz, Michelle , Meleski, Matthew , Sagiv, Ari and Cebe, Peggy(2010) 'Impact of Nanosilicates on Poly(vinylidene fluoride) Crystal Polymorphism: Part 2. Melt-crystallization at Low Supercooling', Journal of Macromolecular Science, Part A, 47: 12, 1208 — 1219
To link to this Article: DOI: 10.1080/10601325.2010.518858
URL: http://dx.doi.org/10.1080/10601325.2010.518858

Journal of Macromolecular Science, Part A: Pure and Applied Chemistry (2010) **47**, 1208–1219

ISSN: 1060-1325 print / 1520-5738 online
DOI: 10.1080/10601325.2010.518858

Taylor & Francis
Taylor & Francis Group

Impact of Nanosilicates on Poly(vinylidene fluoride) Crystal Polymorphism: Part 2. Melt-crystallization at Low Supercooling

B. SEYHAN INCE-GUNDUZ[1], KRISTINA BURKE[2], MICHELLE KOPLITZ[3], MATTHEW MELESKI[2], ARI SAGIV[4] and PEGGY CEBE[1,*]

[1]*Tufts University, Department of Physics and Astronomy, Medford, MA*
[2]*Gallaudet University, Department of Chemistry, Washington, DC*
[3]*Rochester Institute of Technology, Biology Department, Rochester, NY*
[4]*Drexel University, Department of Materials Science and Engineering, Philadelphia, PA*

Nanocomposites of poly(vinylidene fluoride) (PVDF) filled with Lucentite STN^{TM} organically modified silicate (OMS) were investigated upon melt-crystallization at temperatures near its melting point (i.e., at low supercooling temperatures). Previously, we showed that the addition of extremely small amounts of OMS into PVDF causes the polar beta phase formation in cold-crystallized samples, and causes polar gamma phase formation in melt-crystallized samples under high supercooling. The current study focused on the impact of OMS on polymorphic behavior of PVDF crystallized from the molten state, or annealed, at low supercooling temperatures. Nanocomposites with 0–4.0 wt% concentration were prepared from solutions. The existence of α or γ phase was verified by using Fourier transform infrared spectroscopy, wide-angle X-Ray scattering or Differential Scanning Calorimetry (DSC). Morphology of α- and γ-spherulites was observed by polarizing optical microscopy (POM). In annealed PVDF/OMS nanocomposites, gamma crystals were observed to dominate at all clay compositions except 0.01 wt%. DSC and POM data show that two types of gamma crystals, γ and γ', exist when PVDF/OMS nanocomposites were annealed.

Keywords: Nanocomposites, poly(vinylidene fluoride), polymer composite materials, gamma phase

1 Introduction

PVDF is known for its piezoelectric and pyroelectric properties (1–4). PVDF is also of interest due to its crystal polymorphism. Among five different crystallographic phases, the polar beta phase with TTT chain conformation (5) is the origin of the piezoelectric and pyroelectric properties. Beta phase of PVDF usually results from mechanical stretching or rolling of the alpha phase or by application of an electric field (1, 5). Apolar alpha phase, with conformation TGTG' (1, 6), can directly be obtained from melt crystallization (7–10). Another polar phase, gamma, with chain conformation TTTGTTTG' (1, 11), is also obtained usually from the melt or by annealing alpha crystals for a long time at lower supercoolings (12–16). Here, the designation of "high" or "low" supercooling refers to the melt-crystallization temperature range at which neat PVDF exhibits either alpha or gamma crystalline phase, respectively. Besides isothermal crystallization from the melt at elevated temperatures and annealing at high temperatures, other methods to obtain γ-PVDF are casting from solution (17), adding KBr as a nucleating agent (18), or adding organically modified silicates (19).

In previous studies, we investigated the impact of OMS on PVDF under different thermal treatments (19, 20). We observed that new phases emerged and dominated while nanosilicate composition increased in PVDF: beta for cold-crystallized nanocomposites, and gamma for melt-crystallized ones. Upon melt-crystallization, PVDF is known to produce either alpha or gamma depending on its supercooling range (1). The crossover temperature is 155°C, which induces alpha crystal formation at lower temperatures (7–9), and gamma phase forms together with alpha phase when temperature is higher (12–14). For complete 100% gamma PVDF crystals, a sufficient crystallization temperature and/or annealing time is needed (11, 16, 21). Annealing of α-phase PVDF crystals at temperatures close to melting temperature also

*Address correspondence to: Peggy Cebe, Department of Physics and Astronomy, Tufts University, STC-208, 4 Colby Street, Medford, MA 02155. Tel: 617-627-3365; Fax: 617-627-3744; E-mail: peggy.cebe@tufts.edu

produces gamma crystal formations due to a solid-state transformation from alpha to gamma phase (1, 11, 22, 23).

It is known that upon crystallization from the melt at temperatures over 150°C, along with alpha crystals, a second type of spherulite, gamma type, also is obtained (10, 12, 14–16). Highly birefringent alpha spherulites with concentric bands have higher growth rate than gamma spherulites up to a certain temperature (∼167°C for Kynar polymers) above which this situation is reversed (11). Also, for lower temperature crystallization, the slower growth rate of gamma crystals causes the alpha counterparts to surpass gamma spherulites at sufficiently long isothermal crystallization time. Gamma type spherulites have low birefringence due to extensive misorientation of lamellae with respect to the spherulite radius (11). This causes gamma spherulites to be irregular. However, at very high temperatures such spherulites become more regular (11, 13).

Another spherulitic structure of gamma phase, γ'-form spherulites, are produced by solid-state transformation of parts of alpha spherulites (10, 12, 15, 16, 22). Transformation initiates at the junctions of two types of spherulites and grows backwards toward the alpha nucleus, leaving the initial morphology intact. For temperatures 162°C and above, alpha to gamma transformation can also start from the center of alpha spherulites and grow radially (12, 16, 21). Under a polarizing microscope, alpha phase crystals melt first; melt-grown gamma spherulites undergo melting at higher temperatures and gamma crystal parts formed by solid-state transformation of alpha spherulites (γ'-type) melt at the highest temperature (16). The possible alpha to gamma transformation mechanism, i.e., transformation from TGTG' structure to TTTGTTTG', is explained by change of every G-bond to T and of every second G'-bond to G (16, 24).

The treatments to produce gamma crystalline PVDF require very long isothermal crystallization or annealing due to a very low growth rate of gamma type spherulites. We observed in the previous study (19) that organically modified silicates behave as nucleating agent for gamma crystals and we could obtain gamma dominant PVDF by adding OMS nanofillers. In this work, we continued to investigate melt-crystallization of PVDF/OMS nanocomposites at low supercooling temperatures, i.e., temperatures at which neat PVDF exhibits gamma crystalline phase. Nanocomposite samples were prepared either by crystallization from the molten state at 165°C, or by annealing (at 170°C) samples that had been previously melt-crystallized at 150°C.

2 Experimental

2.1 Sample Preparation

The poly(vinylidene fluoride) in pellet form was an Elf Atochem Kynar-based polymer, catalogue number 740. Lucentite STN™, a synthetic smectite clay, was obtained from Zen-Noh Unico, Americas (currently CBC Chemical Company, Japan), as fine powder. Lucentite STN is an organically modified layered silicate prepared by the supplier by ion-exchanging the Na ions in a synthetic smectite clay (Lucentite SWN, with a cation exchange capacity of approximately 0.65 meq/g) for tri octyl methyl ammonium cations (25).

The films of PVDF-OMS nanocomposites were obtained from the mixture of their separate solutions in dimethylacetamide (DMAc) in desired compositions. Solutions were stirred at room temperature for 1–2 days and subsequently mixed in different percentages of OMS, ranging from 0.01% to 4.0% by weight. The mixtures were stirred for several hours at room temperature and after ultra-sonicating for ten minutes they were poured into Petri dishes to dry. Aliquots were reserved for morphological studies. Evaporation of DMAc occurred in about three days sometimes giving a gentle heating to raise the temperature to 70–80°C. Final films were obtained by complete evaporation of DMAc in a vacuum oven. Removal of DMAc solvent was confirmed by thermogravimetric analysis and FTIR. The films were compression molded at 200°C for two minutes, and then quenched into cold water. PVDF films were heated to 210°C in a Mettler hot stage to remove prior thermal history, and then cooled at 20°C/min. and heat-treated using one of two protocols. Films were either: a.) melt-crystallized at 165°C for 16 hours (designated as MC165), or, b.) melt-crystallized at 150°C for one hour (MC150), cooled to room temperature, then annealed at 170°C for 3 hours (ANN170). Both treatments are known to induce the formation of the gamma crystallographic phase in homopolymer PVDF (12–15).

For morphological studies, a droplet of solution from 15 min ultra-sonicated aliquots was placed on a glass cover slip and the same melt crystallization treatment was repeated in the Linkam THMS optical microscope hot stage while observing between crossed polarizers.

2.2 Analysis Methods

Differential scanning calorimetry (DSC) was performed on a TA Instruments 2920 Modulated DSC at a heating rate of 10°C/min from room temperature to 220°C. Heat flow and temperature were calibrated using indium. Endotherms are presented with downward deflection from the baseline. The degree of crystallinity of PVDF was determined from the endotherm area using 104.6 J/g as the heat of fusion of 100% crystalline PVDF (26).

Wide-angle X-ray scattering (WAXS) studies were done using a conventional sealed tube X-ray source having $\lambda =$ 0.1542 nm. A Phillips PW1830 X-ray generator, operated at 40kV and 45ma, and optically encoded diffractometer, were used to investigate the range of scattering angles from $2\theta = 2$–30 degrees (for θ the half-scattering angle). Films were examined in $\theta/2\theta$ reflection mode, using a step scan interval of 0.015 degrees and holding 2.4 seconds per step. D-spacings were calibrated using silicon powder reference

standard placed on the film surface. The PVDF crystal peaks and amorphous halo were modeled using Gaussian wavefunctions, as described previously (20).

For morphology studies, a Nikon Eclipse E600 Polarizing Optical Microscope (POM) with CCD camera was used with the Linkam THMS 600 hot stage unit. Melt-crystallized droplets of PVDF/OMS on glass cover slips were heated to 200°C at 10°C/min to observe melting and subsequently cooled at 20°C/min and crystallized isothermally at 165°C for 16 h. Spherulitic growth and impingement time were monitored under crossed polarizers using long working distance objectives, with camera mounted on the microscope. Static and real-time polarized images of the samples were obtained for different compositions of OMS. The linear growth rate was determined from the slope of spherulite diameter plotted against time.

Infrared studies on bulk films were performed using a Bruker Equinox 55 Fourier Transform infrared spectrometer equipped with an attenuated total reflectance (ATR) cell. A diamond ATR crystal was used to cover the low frequency range from 400–600 cm^{-1}. The resolution was $4cm^{-1}$ and 32 or 256 scans were co-added to improve the signal to noise.

3 Results and Discussion

3.1 Vibrational Spectra

Absorption bands of nanocomposite films of poly(vinylidene fluoride) (PVDF) polymer and organically modified silicates (OMS) prepared at low supercooling temperatures are shown in Figure 1a and 1b. Vibrational spectra are normalized by 1071 cm^{-1} peak as previously suggested (23, 27). Lucentite absorption is observed at 1000 cm^{-1} at highest OMS compositions, i.e., for nanocomposites with 2% and 4% OMS. Nanocomposites isothermally crystallized at 165°C, show more gamma phase when OMS content is greater than 0.032%. At or below 0.032% OMS, alpha phase is dominant and is observed by characteristic frequencies at 532, 613, 764 and 976 cm^{-1} (17, 23). FTIR spectra of nanocomposites with larger amount of OMS do not show significant difference except at frequencies in the range of 400–500 cm^{-1}. At the highest two compositions, 2% and 4%, we observed a growing 444 cm^{-1} band and a broadening on the right side of the peak of 481 cm^{-1}. This might be an indication of some beta phase formation (with beta bands at 444 and 467 cm^{-1}); however, Lucentite OMS itself has absorptions between the mentioned ranges (28). Because we do not see any change in the beta characteristic peak at 1275 cm^{-1} occurring at the same time as the increase for these bands, we assign the increase in absorption at 444 cm^{-1} and 481 cm^{-1} to OMS.

In Figure 1b, annealing causes the crossover composition (from alpha dominant to gamma dominant) to decrease. PVDF with 0%, 0.01%, 0.032%, and 0.05% OMS had more alpha phase absorption than gamma phase when melt-crystallized at 150°C. After annealing at 170°C for 3 h, only neat PVDF and PVDF with 0.01% still had alpha phase dominant. For these two samples, no gamma phase absorption is observed, while for nanocomposites with OMS greater than 0.32%, the alpha phase is nearly absent. The activity in the lowest frequency range 400–500 cm^{-1} is also observed in annealed samples, again probably due to OMS vibrations. Two treatments which produce gamma phase in PVDF/OMS nanocomposites, i.e., 1) melt-crystallization at low supercooling (Fig. 1a); and, 2) annealing close to the melting temperature (Fig. 1b), do not show significant differences in their vibrational spectra. We can conclude annealing is a more effective choice for obtaining gamma phase even with a very tiny amount of OMS, as little as 0.032 wt%.

3.2 Thermal Analysis

Figure 2 shows DSC scans of PVDF-OMS nanocomposites melt-crystallized at 165°C for 16 h, during heating from room temperature to 220°C at 10°C/min. The homopolymer PVDF shows a large endotherm due to melting of alpha crystals at 165.3°C, followed by a smaller endotherm at 180°C due to melting of gamma crystals (1, 12, 22). It should be noted that gamma crystallization is not completed within the isothermal time period; therefore alpha phase crystals were also formed during cooling after crystallization. The addition of OMS to the polymer results in a decrease in the formation of alpha phase crystals and an increase in the gamma phase formation. For low compositions of OMS (i.e., 0% to 0.032%), the alpha crystal endotherm is larger than the gamma endotherm. Therefore, assuming similar heat of fusion for the two crystal forms, the amount of gamma crystals (Table 1) is less than the amount of the alpha crystals at low OMS compositions. In nanocomposites with OMS content equal to or greater than 0.05 wt%, gamma phase starts being dominant, and the alpha crystal melting temperature shifts to lower temperatures, with the endotherm having a broader shape. For example, at 0.1 wt% OMS, the broad peak attributed to the alpha crystal endotherm occurs at 159°C. The gamma phase melting point is relatively stable, shifting upward by 2°C as OMS content increases to 2 wt%. However a smaller shift in melting temperature, of 1°C, was seen in the sample with 4 wt% OMS. This is probably due to a hindering effect of OMS on crystallization at higher OMS concentrations. This behavior is explained by reduced diffusion of chain segments to the growing crystal surface (29). From DSC endotherm data on PVDF/OMS MC165, we conclude that nucleation of gamma phase is enhanced by the addition of Lucentite^{TM} OMS.

It is known that to obtain significant or complete gamma phase in neat PVDF, the isothermal crystallization time should be very long, on the order of days (11, 16, 21). As

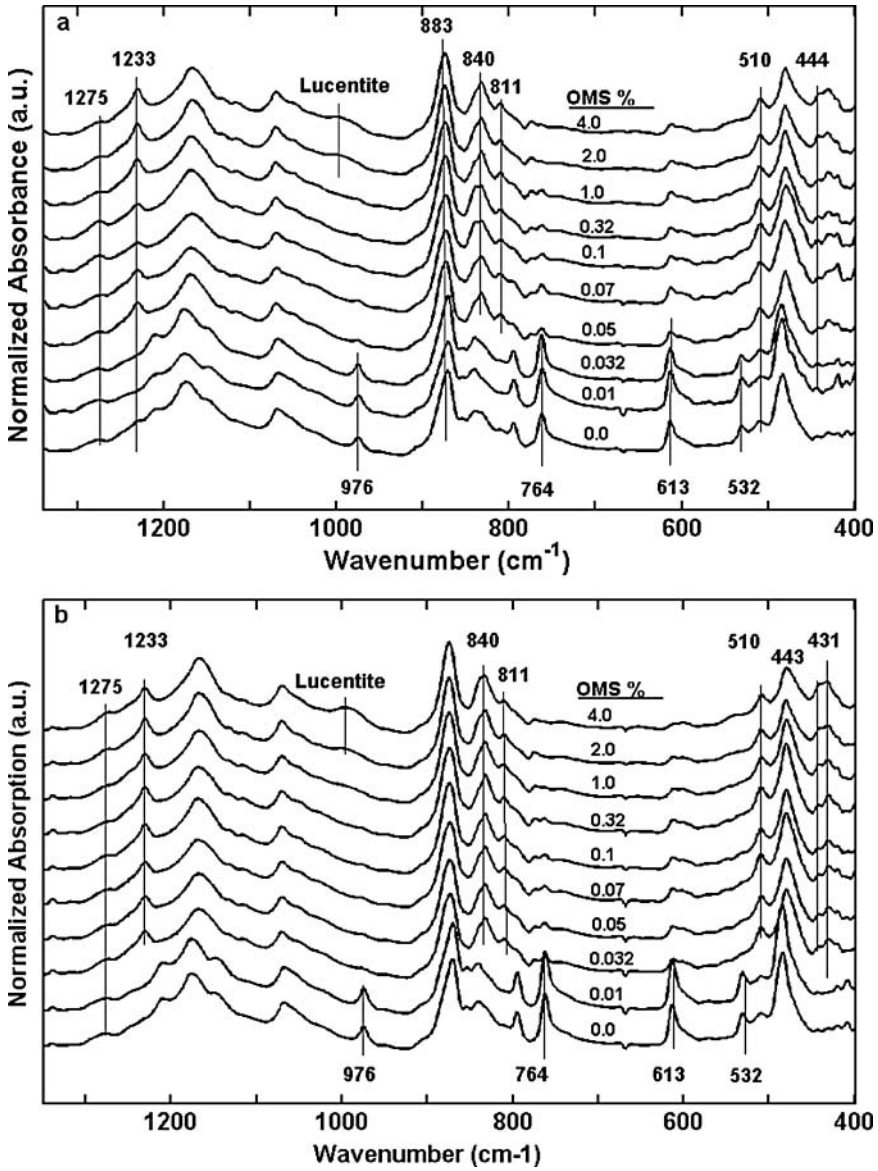

Fig. 1. Normalized infrared absorbance spectra of PVDF/OMS nanocomposites prepared by: a) crystallization from the melt at 165°C for 16 h, and b) annealing the samples, previously melt-crystallized at 150°C for 1 h, at 170°C for 3 h. OMS compositions are indicated, and several prominent bands for alpha and gamma phases are marked.

Table 1. Thermal properties of melt crystallized PVDF/OMS nanocomposites[#] : area of melting endotherm and peak and final melting temperatures

OMS (%)	*ΔH (J/g) (±2.0)*	*Tm_1 (C) (±0.3)*	*Tm_2 (C) (±0.3)*	*Tm_3 (C) (±0.3)*	*T_{final} (C) (±0.3)*
0.0	56.8	165.3	167.4	180.6	193.6
0.01	54.0	164.0	167.4	180.9	186.9
0.032	50.1	164.2	Sh*	180.6	186.9
0.05	53.1	159.3	170.0	181.2	189.0
0.07	58.1	159.3	169.9	181.1	187.0
0.1	58.1	159.1	169.9	181.2	190.8
0.32	50.2	157.6	170.3	181.1	188.0
1.0	61.0	156.6	None	181.8	188.7
2.0	50.7	161.1	None	182.6	191.9
4.0	51.9	154.7	None	181.0	188.3

[#]Samples were melt crystallized at 165°C for 16 h, and then heated from room temperature to 220°C at 10°C/min.
*Sample 0.032% displayed an unresolved shoulder (Sh) on the higher temperature side of Tm_1.

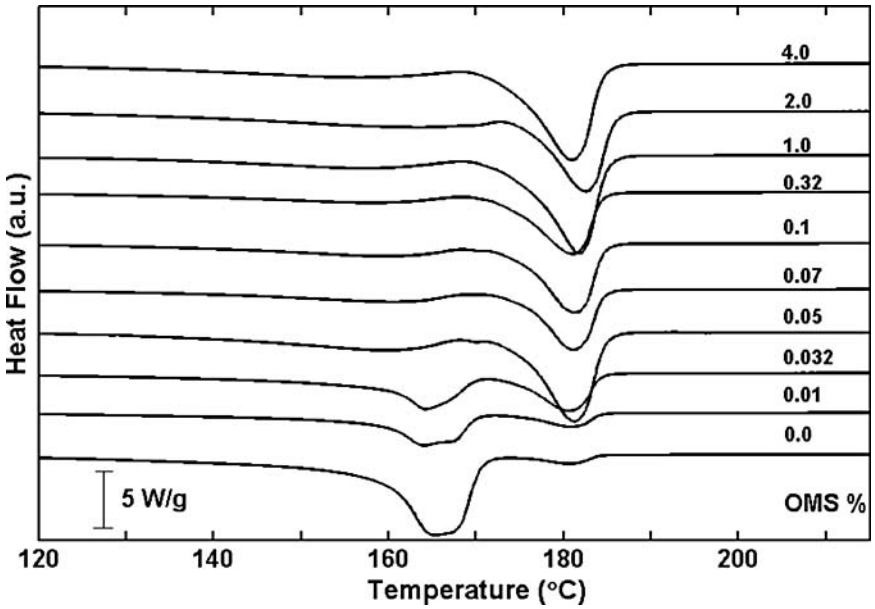

Fig. 2. Normalized heat flow vs. temperature during DSC scanning at 10°C/min, shown from 120°C to 215°C, for PVDF/OMS nanocomposites melt crystallized at 165°C for 16 h. OMS compositions are indicated. Heat flow is normalized for sample mass.

also observed in a previous study (19), isothermal crystallization from the molten state in the presence of organically modified silicates triggers gamma crystal formation significantly. We can conclude that OMS can be used as a nucleation agent for obtaining a significant amount of gamma phase crystals in a PVDF matrix.

Figure 3a, b shows the DSC heating curves of MC150 nanocomposites, respectively, before and after, annealing at 170°C for 3 h. Before annealing, PVDF without any nanofiller shows two alpha-melting endotherms with a major one at 169°C and a broad one at 156°C attributed to less perfect alpha crystals formed during cooling after crystallization. With OMS addition into PVDF, another endotherm appears at 174°C indicating gamma crystal formation. At the highest OMS composition, 4%, the alpha melting peak becomes very broad and merges with a significant gamma crystal endotherm. Readers are referred to reference (19) for details on the DSC curves of the MC150 samples. When annealed, the broad peak at 156°C disappears in neat PVDF and two melting points are observed at 164.7°C and at 167.4°C, as well as a small peak at 184.3°C. The first at 164.7°C is probably due to annealing of imperfect crystals having T_m at 156°C before annealing. The second melting endotherm at 167.4°C is due to alpha crystals formed during melt-crystallization at 150°C. The tiny melting peak occurring at 184.3°C can be attributed to gamma crystals formed by transformation from alpha crystals. DSC data are listed for MC165 and ANN170 nanocomposites in Tables 1 and 2 for an area of the total endotherm, ΔH, melting temperature peaks in increasing order, T_{m1}, T_{m2} and T_{m3}, and the temperature where melting ends completely, $T_{m-final}$.

Table 2. Thermal properties of annealed PVDF/OMS nanocomposites[#] : area of melting endotherm and peak and final melting temperatures

OMS (%)	*ΔH (J/g) (±2.0)*	*Tm_1 (C) (±0.3)*	*Tm_2 (C) (±0.3)*	*Tm_3 (C) (±0.3)*	*T_{final}(C) (±0.3)*
0.0	54.0	164.7	167.4	184.3	186.8
0.01	49.3	165.4	179.4	181.5	187.4
0.032	55.2	163.3	178.8	181.5	188.7
0.05	49.4	167.5	178.5	182.5	190.4
0.07	55.8	163.2	178.5	181.4	190.8
0.1	54.4	162.1	178.9	181.5	188.4
0.32	53.9	162.1	179.4	182.6	192.2
1.0	44.6	154.1	179.6	181.3	188.0
2.0	50.5	170.4	none	184.2	191.9
4.0	47.7	172.4	none	183.9	189.7

[#]Samples were melt crystallized at 150°C for 1 h, subsequently annealed at 170°C, and then heated from room temperature to 220°C at 10°C/min.

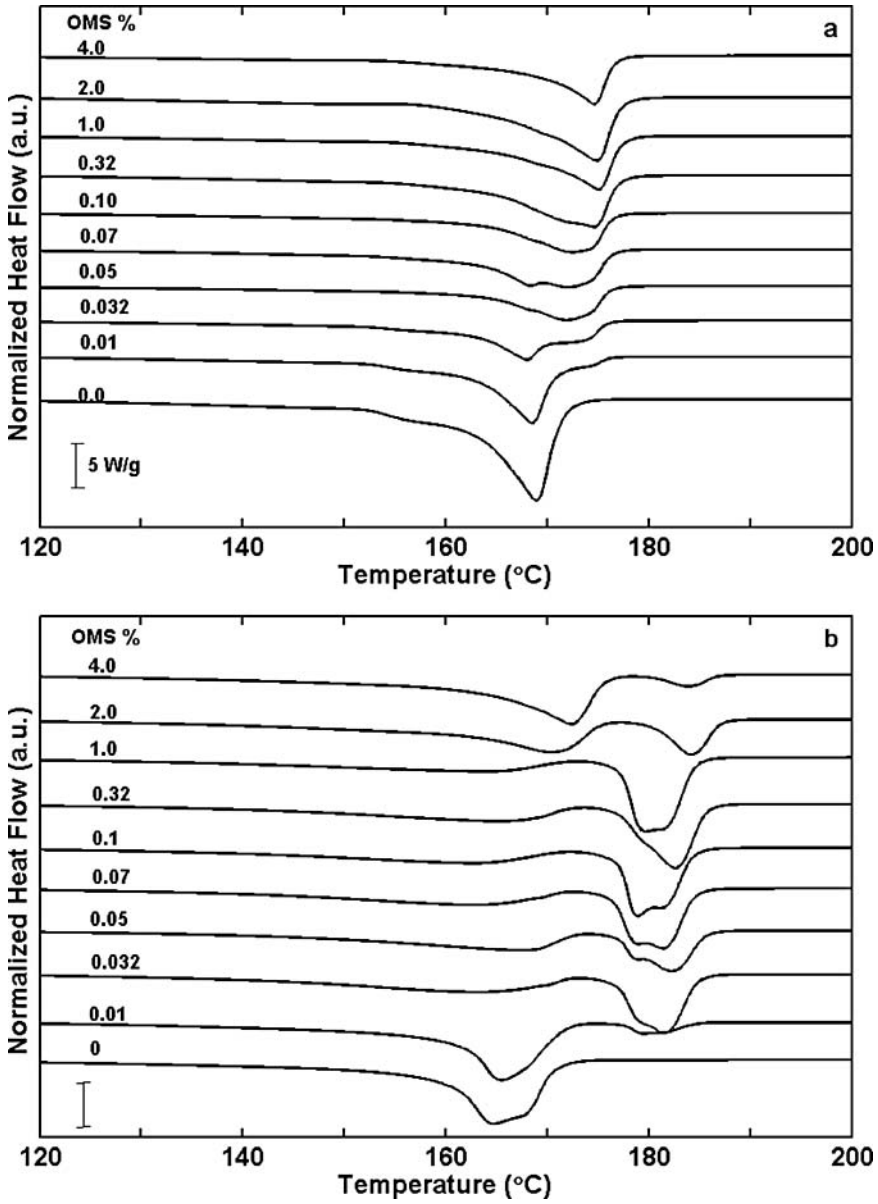

Fig. 3. Heat flow vs. temperature during DSC scanning at 10°C/min, shown from 120°C to 200°C, for PVDF/OMS nanocomposites: a) crystallized at 150°C for 1 h, b) annealed at 170°C for 3 h after treatment in (a) OMS compositions are indicated. Heat flow is normalized for sample mass.

At higher OMS content, alpha crystal endotherms broaden and shift to lower temperatures. The gamma crystal phase endotherm observed at 0.01 wt% OMS occurs at 181.5°C and the endotherm area steadily increases until the OMS content reaches 0.32% by weight. Once again, the shift to higher melting temperatures was observed in PVDF/OMS nanocomposites with higher OMS content. The highest gamma crystal melting is observed to occur at 184°C in the 2 wt% and 4 wt% OMS nanocomposites. Melting of gamma crystals shows a double peak due to formation of two types of gamma crystals, γ and γ'. The first is due to the melt-crystallization at 150°C and the second type is known to be formed by transformation of alpha crystals. When OMS content in PVDF increases, the endotherm area of gamma crystals formed by transformation decreases. This is in accordance with less alpha crystal formation in nanocomposites before annealing as OMS fraction increases. However, when OMS content increases above 1 wt%, the gamma phase endotherm area starts to decrease in favor of an increase in a new endotherm occurring at a temperature between the alpha and gamma melting points. This endotherm is observed for 2 wt% OMS and 4 wt% OMS samples at 170.4°C and 172.4°C, respectively. In other techniques, FTIR and WAXS, we have not observed any new phase formation for nanocomposites with OMS over 1 wt% that could account for this peak.

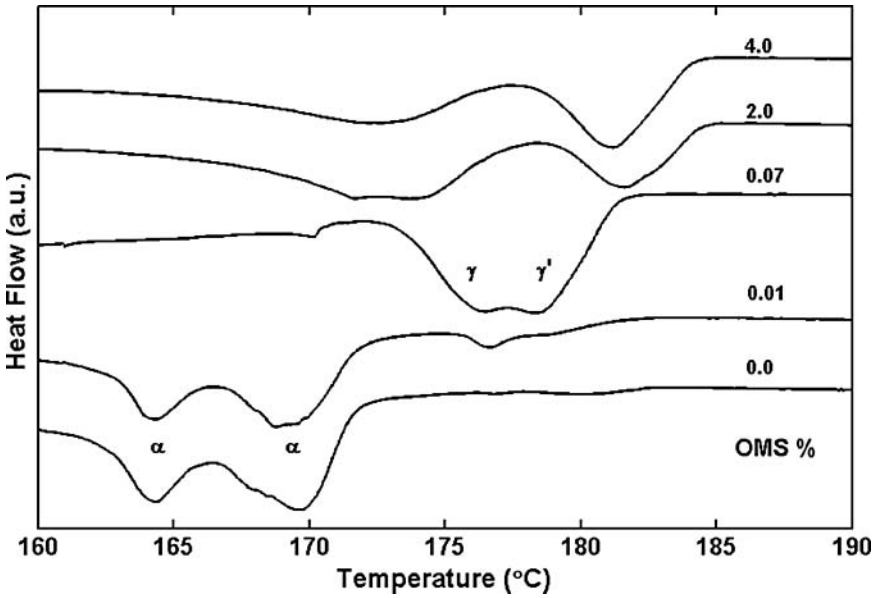

Fig. 4. Normalized heat flow vs. temperature of MC150 PVDF/OMS nanocomposites after annealing at 170°C. Samples were heated from 150°C to 200°C at a rate 1°C/min. Normalization is made for both sample mass and OMS content.

For a closer observation of melting behavior of PVDF/OMS nanocomposites we applied a slow heating to selected compositions from 150°C to 200°C, at a rate of 1°C/min. As seen in Figure 4, two alpha endotherms that were merged in Figure 3b, could be resolved as two separate peaks for nanocomposites with 0% or 0.01% OMS. The first T_m is observed at 164.5°C and the latter is at 170°C. In PVDF with no clay content, the higher melting endotherm resulting from alpha to gamma conversion could be slightly seen at 181°C. For PVDF with 0.01% OMS, two melting peaks are seen on the higher temperature side, at 176.5°C and 179°C, for γ and γ' crystal melting, respectively. γ'-crystal melting started to be dominant at 0.07% OMS as previously shown. For this sample, the alpha endotherm is very small, probably due to a better re-organization of gamma crystal at high temperatures during slow heating.

The new endotherm observed in Figure 3b, for nanocomposites with 2 and 4% OMS, occurs in the slowly heated samples (Fig. 4) at slightly higher temperatures, 173.6°C and 172.8°C, respectively. The lower temperature endotherm can be a result of retardation of crystallization due to higher OMS content and its hindering effect (29), which was observed previously (20). Gamma crystals, which are formed under the hindering effect of OMS before annealing, melt at lower temperatures. The high temperature melting, which was seen around 184°C before annealing, is now observed at 181°C for these two highest compositions. Also an increase in area of melting is observed at 4% PVDF/OMS nanocomposite sample. The endotherm at higher temperature is probably a result of annealing under which crystal re-organization causes crystals to become perfected to some extent. Readers should be reminded that there is almost no alpha phase indication in the 150°C melt-crystallized samples for these nanocomposites, and therefore a transformation from alpha to gamma is negligible.

3.3 Wide-Angle X-ray Scattering

Figure 5a, b shows composite WAXS intensity vs. two theta plots of PVDF nanocomposite melt-crystallized samples at low supercoolings. Figure 5a includes the samples isothermally crystallized from the melt at 165°C for 16 h. WAXS scans for the samples annealed at 170°C after melt-crystallization at 150°C are shown in Figure 5b. The two figures show closely similar WAXS behavior occurs as OMS content increases. Alpha crystal phase reflections could be seen clearly in neat PVDF (the two bottom plots). Alpha crystal peaks with d-spacings $d_{100}(\alpha) = 0.49$ nm, $d_{020}(\alpha) = 0.48$ nm , $d_{110}(\alpha) = 0.44$ nm , and $d_{021} = 0.33$ nm are represented at $2\theta = 17.6, 18.3, 19.9$ and 26.5 degrees, respectively (6, 30). Among them, the (100) peak is the unique alpha reflection while the remaining ones overlap with gamma crystal reflections. Gamma reflections of (020), (110) and (022) planes overlap with alpha peaks with Miller indices (020), (110) and (021), respectively (19, 31). Also, gamma crystals have another peak, (021), which overlaps with the beta reflection of (200)/(110). In Figure 5, the (100) alpha peak disappears for nanocomposites with greater than 0.05% OMS. Upon adding OMS clay to PVDF, the major (110) alpha peak at $2\theta = 19.9$ degrees shifts to higher angle, $2\theta = 20.1$ degrees, and is replaced with a broader peak. This is due to the growth of gamma peaks with d-spacings $d_{110}(\gamma) = 0.442$ nm and $d_{021}(\gamma) = 0.431$nm overlapping with the major alpha peak. For the lowest two clay contents, 0.01% and 0.032%, gamma reflection is observed as a shoulder on the (110) alpha peak. Due to disappearance of

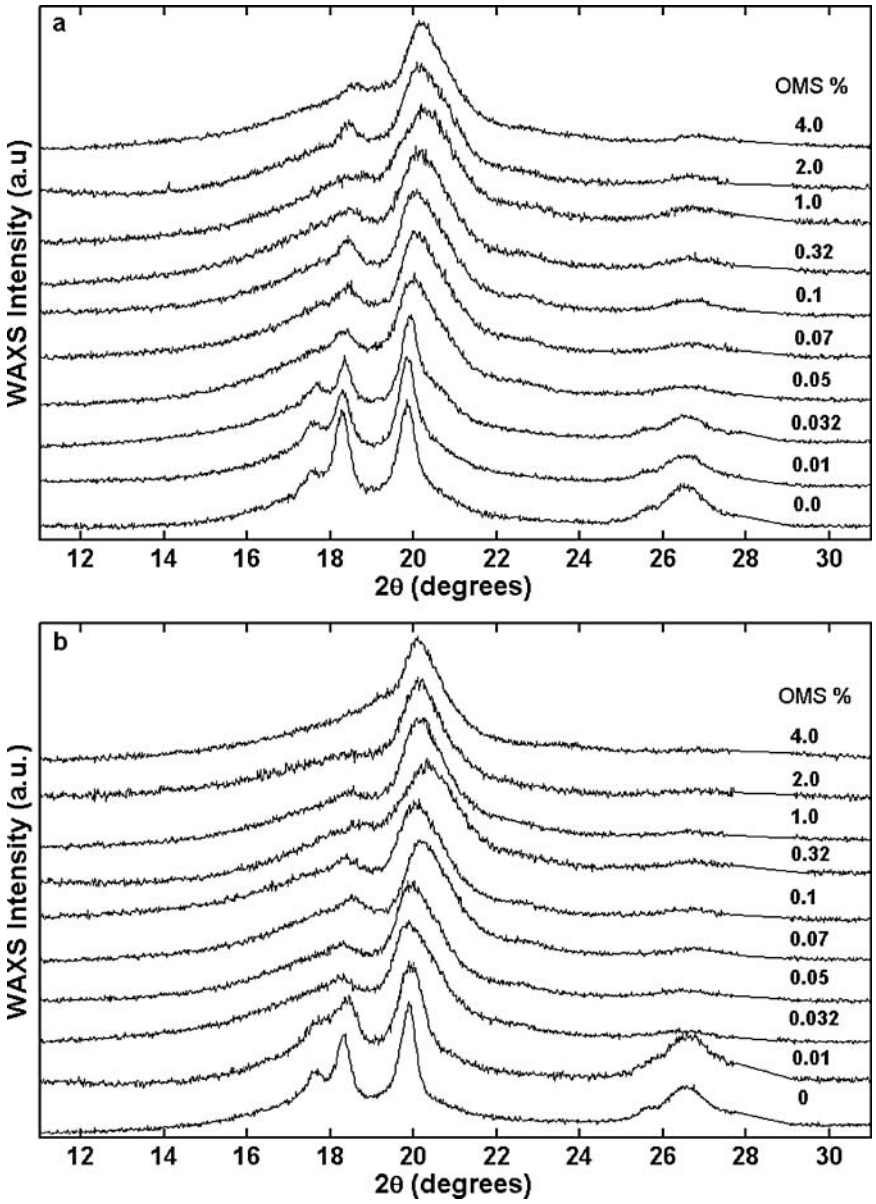

Fig. 5. Wide-angle X-ray scattering intensity vs. two theta ($\lambda = 0.1542$ nm) at room temperature, for PVDF/OMS nanocomposites: a) melt-crystallized at 165°C for 16 h; b) melt-crystallized at 150°C for 1 h and then annealed at 170°C for 3 h. OMS compositions are indicated. Near $2\theta = 28.4$ degrees, the Si reference standard peak has been deleted and replaced by a straight line, to facilitate subsequent Gaussian curve fitting.

the reflection from the $d_{100}(\alpha)$ planes, other gamma crystal reflections (020) and (022) are assumed to be dominant for nanocomposites with 0.05% OMS and greater. The weak but unique gamma phase diffraction plane (111) could be seen around $2\theta = 22.6$ degrees with a d-spacing of 0.39 nm (32). This unique reflection from $d_{111}(\gamma)$ first becomes visible in the nanocomposite with 0.05% OMS by weight in 165°C melt-crystallized samples. Using Gaussian fitting we were able to fit a tiny beta peak for 1% OMS and higher, although quantitatively we were not able to measure the fraction.

WAXS data show only a slight difference when comparing the annealed nanocomposites of samples previously melt-crystallized at 150°C, and the MC165 samples. Alpha crystal plane reflection of (100) is observed only in 0.01 wt% nanocomposite and homopolymer diffraction patterns. The gamma (111) peak starts to appear at a slightly lower OMS composition of 0.032 wt% in the MC150 samples annealed at 170°C. In both figures, $d_{111}(\gamma)$ peak does not change significantly up to 4 wt% OMS. Replacement of (020) and (110) alpha peaks are seen once more as OMS concentration increases.

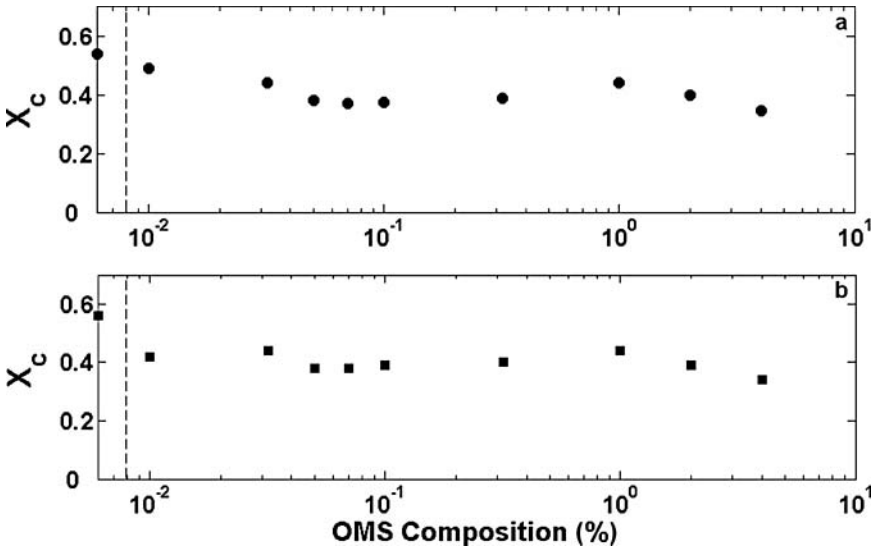

Fig. 6. Crystallinity index vs. OMS composition, for PVDF/OMS nanocomposites: a) melt-crystallized at 165°C for 16 h, and b) melt-crystallized at 150°C for 1 h and then annealed at 170°C for 3 h.

Figure 6 shows total crystallinity index vs. OMS composition on a logarithmic scale, calculated from Gaussian fitting of the crystal peaks, as described previously (20). For comparison purposes homopolymer PVDF data are placed at an arbitrary x-position on the left of the plot. For the samples melt-crystallized at 165°C (Fig. 5a), the crystal weight fraction in homopolymer PVDF is 0.52 and it decreases to 0.34 when OMS content reaches 4 wt%. Samples annealed at 170°C (Fig. 5b), show a very similar behavior having 0.56 crystal fraction in neat PVDF, decreasing to 0.34 in the PVDF/OMS nanocomposites with highest OMS content. As remarked in previous papers

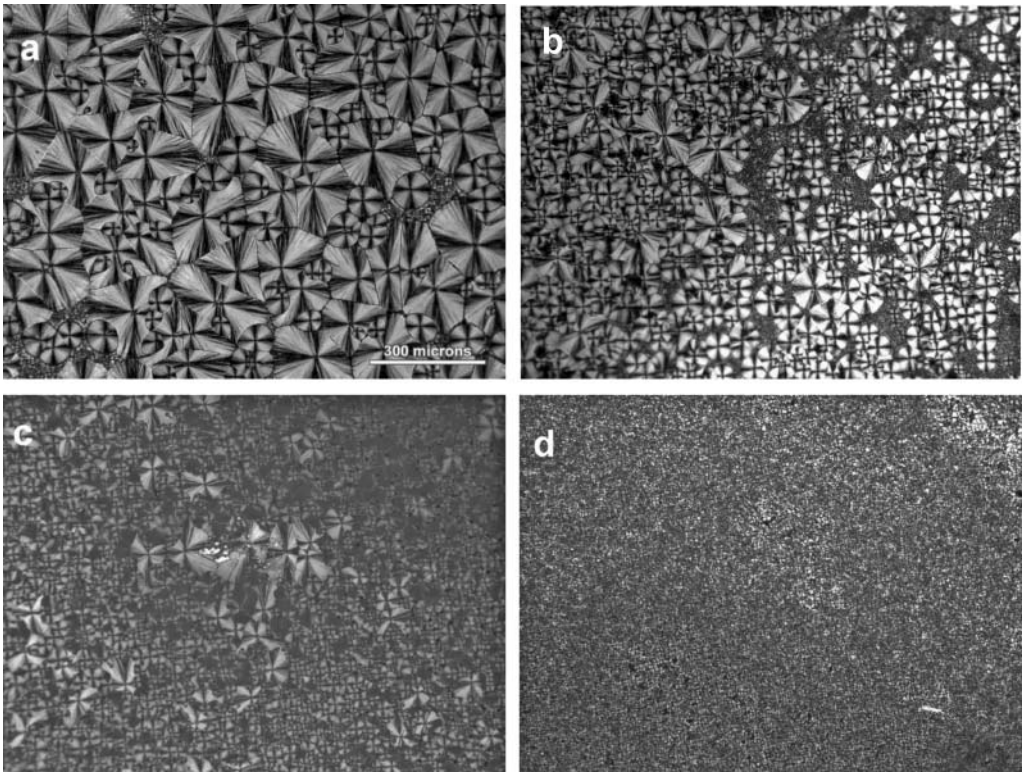

Fig. 7. POM images of melt-crystallized PVDF/OMS nanocomposites crystallized at 165C for 16 h. OMS compositions by weight: a) 0.0, b) 0.032, c) 0.07, and d) 0.32. The scale bar in (a) applies for all images.

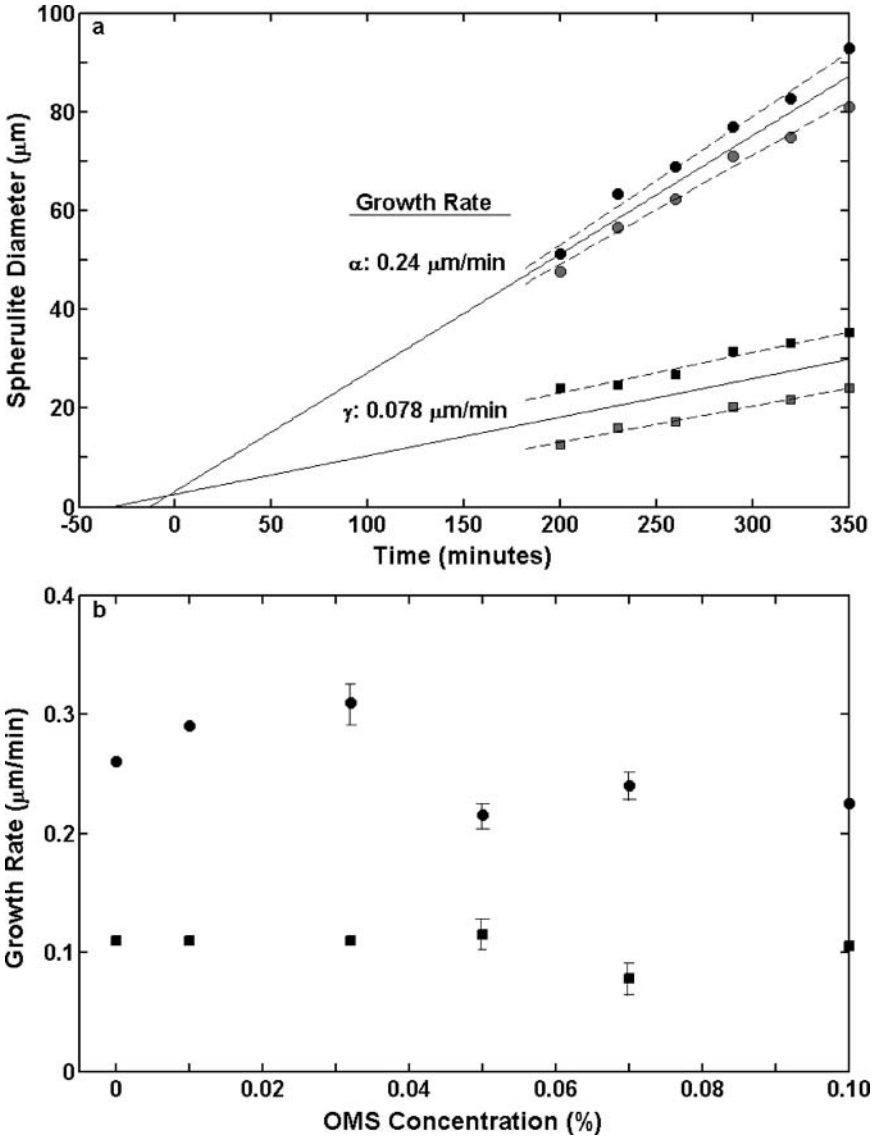

Fig. 8. a) Spherulite diameter vs. time during melt crystallization at 165°C, for highly birefringent alpha spherulites (circles), and gamma spherulites (squares) in PVDF nanocomposites with 0.07% OMS. The diameters of a few spherulites of each type were tracked for each time and the fitted line is drawn using average points; b) Growth rates of alpha (circles) and gamma (squares) spherulites vs. OMS composition by weight. Gamma phase spherulites grow 2–3 times more slowly than their alpha counterparts.

(19, 20) on cold-crystallization and melt-crystallization of PVDF/OMS nanocomposites, for the samples crystallized or annealed at low supercoolings, the impact of OMS addition is also to retard crystallization due to hindered chain mobility (29). We were not able to quantify alpha, beta, and gamma crystals amounts separately due to irresolution of their diffraction peaks.

3.4 Polarizing Optical Microscopy (POM)

The morphology of MC165 nanocomposites observed by POM shows complex behavior, as seen in Figure 7a-d. Homopolymer PVDF (Fig. 7a) clearly shows alpha and gamma spherulites coexisting. The small, weakly birefringent spherulites with a distorted oval shape are gamma spherulites (1). Larger spherulites with concentric bands are initially nucleated as alpha crystals during isothermal crystallization, and they subsequently start to transform to gamma phase as crystallization time increases. Also, small coarse gamma spherulites nucleate and grow during isothermal crystallization separately from the transforming alpha spherulites. These two different types of gamma spherulites are known to melt at different temperatures as we also observed with POM (Table 3). Small coarse gamma spherulites melt completely at 185°C, while large and banded gamma spherulites melt at 192°C agreeing with literature (16, 21). Tiny, irregular spherulites seen between the two types of gamma spherulites are alpha phase

Table 3. Final melting temperatures from POM of alpha and gamma spherulites grown at 165°C

OMS, %	*$\alpha - T_m$ (°C) (±0.3)*	*$\gamma - T_m$ (°C) (±0.3)*	*γ'-T_m (°C) (±0.3)*
0	172	185	193
0.01	172	186	194
0.032	172	186	193
0.05	172	187	194
0.07	172	186	193
0.10	none*	185	193

*Unable to detect alpha spherulites

spherulites, which are formed during cooling after isothermal crystallization time completed. POM images taken during melting confirm their alpha phase character showing that complete melting occurs by 167°C.

An example of the growth rate of small coarse gamma spherulites and large crystals (which were alpha phase crystals at the beginning growing radially) is shown in Figure 8a. Small crystals nucleate at an earlier time but grow more slowly than their neighbors. This causes segregated regions of small and large spherulite populations, and their larger alpha counterparts eventually envelop the small coarse gamma spherulites. In Figure 8a, extrapolation of growth rate shows nonzero diameter at zero time scale. This could be due to a time lag between the beginning of image recording and the isothermal crystallization time. Another possibility is nucleation of spherulites just before the temperature reaches 165°C, while the hot stage is stabilizing its temperature from cooling state to isothermal state. Growth rates of different PVDF/OMS nanocomposites also are shown in Figure 8b. Growth rate does not show any significant change at different OMS compositions, for either gamma or alpha spherulites. On the other hand, the small coarse gamma spherulites grow approximately three times slower than alpha spherulites. Growth rates of PVDF spherulites for the applied crystallization temperature agree well with the literature (11, 33).

When Lucentite OMS is added to PVDF an irregularity in the spherulites is observed. At 0.032 wt% OMS small gamma type spherulites become more frequent and some spherulites with irregular birefringence start to appear. The reasons for formation of this type of spherulites, with a dark interior part, are not known but have been reported in the literature (12, 21). Prest and Luca named those spherulites, with irregular birefringence having complete circular shape, as "wagon-wheel" shaped spherulites (12). In PVDF/OMS nanocomposites, wagon-wheel texture is seen mostly in association with some part of α spherulites which truncates their shape; we rarely observed full "wheeled" spherulites. As OMS content increases, regions with no apparent birefringence increase, probably due to occurrence of this type of spherulites. For 0.32 wt% and greater, spherulites are too tiny to be resolved by POM due to the nucleation effect of Lucentite.

Final melting temperatures of three types of spherulites α, γ, and γ' are listed in Table 3. No significant difference was observed with respect to OMS composition for each spherulite type.

4 Conclusions

Our study of PVDF/OMS nanocomposites, melt-crystallized at low supercoolings, shows that OMS plays a role as a gamma nucleation agent in PVDF polymer, which we also observed in nanocomposites with crystals melt-grown at high supercoolings (19). Nanocomposites annealed at 170°C after a melt-crystallization at 150°C, and PVDF/OMS samples melt-crystallized at 165°C, do not show significant differences in FTIR and WAXS analysis. However, gamma nucleation is observed at slightly lower OMS compositions in the annealed nanocomposites.

DSC results show gamma crystals dominate in MC165 nanocomposites for OMS content greater than 0.032%. In ANN170 samples, gamma phase melting endotherm is observed being dominant for OMS content at and above 0.032%. Annealed samples showed two gamma melting points due to formation of two types of gamma crystals, those formed during either isothermal crystallization or by solid-state transformation from pre-existing alpha crystals.

Morphology of melt-crystallized PVDF/OMS nanocomposites at 165°C showed an irregular pattern with addition of Lucentite OMS. Spherulites with irregular birefringence increased with OMS content. Upon their melting, three different melting temperature were observed representing α-type, γ-type, and γ'-type spherulites.

To conclude, the addition of OMS to PVDF results in a decrease in the formation of alpha crystals and an increase in the gamma phase formation. OMS can be used as a nucleation agent for obtaining a significant amount of gamma phase crystals in a PVDF matrix. Annealing at temperatures close to melting point is a more effective choice for obtaining gamma phase even with a very tiny amount of OMS, as little as 0.032 wt%.

The impact of OMS on crystalline modification and crystal kinetics is, and will continue to be, an important issue for many semicrystalline polymers. New and emerging technologies that use polymers and biopolymers which may be difficult or slow to crystallize (for example, poly(butylene terephthalate) and poly(lactic acid)), may benefit from the addition of OMS. Commercialization of polymers containing OMS will require detailed study of the impact of nanoparticle additives on the crystalline phase structure and kinetic development, such as we have shown here for PVDF.

Acknowledgments

The authors thank the National Science Foundation, Polymers Program of the Division of Materials Research, for

support of this research through grant DMR-0406127. Undergraduate summer interns Burke, Koplitz, Meleski, and Sagiv performed the research reported herein at Tufts University. A portion of the X-ray scattering work was conducted at the Brookhaven National Laboratory, National Synchrotron Light Source, Advanced Polymers Beamline X27C supported by the Department of Energy.

References

1. Lovinger, A.J. (1982) Poly(vinylidene fluoride). In Developments in Crystalline Polymers–1. Bassett, D.C., Ed. Applied Science Publishers: London.
2. Davies, G.R. (1980) Physics of Dielectric Solids. In Inst. Phys. Conf. Series No. 58. Goodman, C., Ed.
3. Broadhurst, M.G., Davis, G.T. and McKinney, J.E. (1978) *J. Appl. Phys*., 49, 4992.
4. Kepler, R.G. and Anderson, R.A. (1978) *J. Appl. Phys*., 49, 4490.
5. Hasegawa, R., Takahashi, Y., Chatani, Y. and Tadokoro, H. (1972) *Polym. J*., 3, 600.
6. Bachmann, M. and Lando, J. (1981) *Macromolecules*, 14, 40.
7. Nakamura, S., Sasaki, T., Funamoto, J. and Matsuzaki, K. (1975) *Makromol. Chem*., 176, 3471.
8. Mancarella, L. and Martuscelli, E. (1977) *Polymer*, 18, 1240.
9. Welch, G.J. and Miller, R.L. (1683) *J. Polym. Sci. Polym. Phys. Ed*., 14, 1683.
10. Gianotti, G., Capizzi, A. and Zamboni, V. (1973) *Chim. Ind*., 55, 501.
11. Lovinger, A.J. (1980) *J. Polym. Sci. Polym. Phys. Ed*., 18, 793.
12. Prest, W.M. Jr. and Luca, D.J. (1975) *J. Appl. Phys*., 46, 4136.
13. Lovinger, A.J. and Keith, H.D. (1979) *Macromolecules*, 12, 919.
14. Morra, B.S. and Stein, R.S. (1982) *J. Polym. Sci. Polym. Phys. Ed*., 20, 2243.
15. Osaki, S., and Ishida, Y. (1975) *J. Polym. Sci. Polym. Phys. Ed*., 13, 1071.
16. Lovinger, A.J. (1980) *Polymer*, 21, 1317.
17. Kobayashi, M., Tashiro, K., and Tadokoro, H. (1975) *Macromolecules*, 8, 158.
18. Miyazaki, T., Takeda, Y., Akasaka, M., Sakai, M., and Hoshiko, A. (2008) *Macromolecules*, 41, 2749.
19. Ince-Gunduz, B.S., Alpern, R., Amare, D., Crawford, J., Dolan, B., Jones, S., Kobylarz, R., Reveley, M. and Cebe, P. (2010) *Polymer*, 51(6), 1485–1493.
20. Buckley, J., Cebe, P., Cherdack, D., Crawford, J., Ince, B.S., Jenkins, M., Pan, J., Reveley, M., Washington, N. and Wolchover, N. (2006) *Polymer*, 47, 2411–2422.
21. Gregorio, R. Jr. and Capitao, R.C. (2000) *J. Mater. Sci.*, 35, 299.
22. Prest, W.M. Jr. and Luca, D.J. (1978) *J. Appl. Phys*., 49, 5042.
23. Bachmann, M.A. and Gordon, W.L. (1979) *J. Appl. Phys*., 50, 6106.
24. Takahashi, Y. and Tadokoro, H. (1980) *Macromolecules*, 13, 1317.
25. CBC Co. Ltd, Tokyo, Japan. http://www.cbc.co.jp/indexe_n.html
26. Nakagawa, K. and Ishida, Y. (1973) *J. Polym. Sci. Part B: Polym. Phys*., 11, 2153.
27. Benz, M. and Euler W.B. (2003) *J. Appl. Polym. Sci*., 89, 1093.
28. Ramasundaram, S., Yoon, S., Kim, K.J. and Park, C. (2008) *J. Polym. Sci. Part B: Polym. Phys*., 46, 2173.
29. Lochhead, R.Y. and Boykin, C.M. In Polymer nanocomposites: synthesis, characterization, and modeling, Washington, DC, American Chemical Society; 2002; ACS Symposium Series 804, 85–98.
30. Lando, J.B., Olf, H.J. and Peterlin, A. (1966) *J. Polym. Sci. Part A-1*, 4, 941.
31. Gregorio, R. Jr. (2006) *J. Appl. Polym. Sci*., 100, 3272–3279.
32. Lovinger, A.J. (1981) *Macromolecules*, 14, 322.
33. Penning, J.P. and St. John Manley, R. (1996) *Macromolecules*, 29, 84.